

Dalton Transactions

Accepted Manuscript



This is an *Accepted Manuscript*, which has been through the Royal Society of Chemistry peer review process and has been accepted for publication.

Accepted Manuscripts are published online shortly after acceptance, before technical editing, formatting and proof reading. Using this free service, authors can make their results available to the community, in citable form, before we publish the edited article. We will replace this *Accepted Manuscript* with the edited and formatted *Advance Article* as soon as it is available.

You can find more information about *Accepted Manuscripts* in the [Information for Authors](#).

Please note that technical editing may introduce minor changes to the text and/or graphics, which may alter content. The journal's standard [Terms & Conditions](#) and the [Ethical guidelines](#) still apply. In no event shall the Royal Society of Chemistry be held responsible for any errors or omissions in this *Accepted Manuscript* or any consequences arising from the use of any information it contains.

Cite this: DOI: 10.1039/c0xx00000x

www.rsc.org/xxxxxx

ARTICLE TYPE

Theoretical insights into the effect of amine and phosphine decoration on the photoluminescence of copper(I) and silver(I) coordination polymers

Craig A. Bayse,^{*a} Lenora K. Harper,^{a,b} Jasprina L. Ming^a and Robert D. Pike^b

⁵ Received (in XXX, XXX) Xth XXXXXXXXX 20XX, Accepted Xth XXXXXXXXX 20XX
DOI: 10.1039/b000000x

Coinage metal cyanides (MCN) form photoluminescent 1D coordination polymers. The decoration of these chains with amine and phosphine ligands shifts the wavelength for photoluminescence into the visible region. Density-functional theory (DFT) and time-dependent DFT (TD-DFT) calculations of zigzag and helical models of decorated chains are used to show that the transitions that contribute to the experimental spectra are related to the π - π excitations previously shown for coinage metal cyanide chains.

Introduction

Coinage metal cyanides (MCN) form photoluminescent 1D coordination polymers¹⁻⁶ that readily react with Lewis bases, such as aliphatic and aromatic amines and phosphines, to form 1D, 2D or 3D decorated coordination polymers or molecular compounds.⁷ MCN itself consists of infinite chains of MCN units, often with disorder in the orientation of the CN units. A wide variety of ligand-decorated MCN compounds and materials have been synthesized, with the 1:1 ratio of metal to ligand (L) being most common.⁸⁻²⁶ For decorated Cu(I) networks, the metal centres tend to be three-coordinate with one ligand bonded to each metal centre, although examples of alternating 2/4-coordinate of CuCN(P(OPh)₃), AgCN(PAr₃) and {Ag,Cu}CN(PAr₃) materials have been reported.^{27,28} Fewer examples of ligand-rich (M:L < 1:1) and ligand-deficient (M:L > 1:1) materials have been synthesized. The former tend to be found for L = aromatic amine or mixed phosphine/aromatic amine due to the low stabilization energy for coordination of a fourth ligand to Cu(I).^{10,14} Ligand-deficient networks include both 2- and 3-coordinate metal centres and have been reported for pyridine derivatives, nitriles, and bulky phosphines.^{29,30} Relatively fewer molecular compounds are known; an example is CuCN(MeIm)₃,¹⁰ which contains a terminal CN ligand. Molecular AgCN-derived compounds sometimes include short undecorated fragments of the MCN polymer.³¹ More complex materials containing both decorated and undecorated MCN chains are also known, e.g. 4[CuCN(Pyr)]·3[CuCN] (Pyr = pyridine).¹⁰ CuCN coordination polymers have been recently reviewed.⁷

Interestingly, many of these MCN-L complexes are photoluminescent, showing red-shifted emission versus that of the undecorated materials (CuCN: 392 nm; AgCN: 399 nm).³² A few MCN-L complexes, including certain ligand-rich species,

such as CuCN(Pyr)₂ and those with *p*-substituted-Pyr ligands, are non-emissive. Our experimental studies have shown that simple exposure of liquid or gaseous amine causes the emission of bulk CuCN to move into the visible region (see Fig 1).³³ Remarkable differences in emission wavelengths are found for closely related ligands in some cases. X-ray diffraction studies have demonstrated that short-duration ligand exposure of CuCN produces CuCN-L as a surface phase with the bulk material remaining unchanged. The fact that CuCN spontaneously reacts with a wide range of nucleophiles producing emissive products at a variety of response wavelengths is suggestive of the potential that CuCN could function as a luminescence detector for nucleophiles.³³

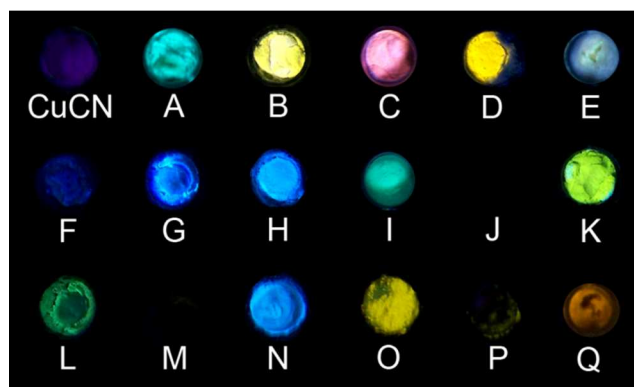


Fig 1. Luminescence of CuCN + liquid L under 254 nm light at room temperature. A: Piperidine (Pipd) B: N-MePipd, C: N-Et-Pipd, D: N-MePyrrolidine, E: Me₂NCy, F: NEt₃, G: N-methylmorpholine, H: N-methylpiperazine (N-MePipz), I: N,N'-Me₂Pipz, J: Pyr, K: 2-MePyr, L: 3-MePyr, M: 4-MePyr, N: 2-EtPyr, O: 3-EtPyr, P: 4-EtPyr, Q: 4-^tBuPyr. (reprinted with permission from Chemical Communications **2010**, *46*, 4565–4567; copyright 2010 Royal Chemical Society).

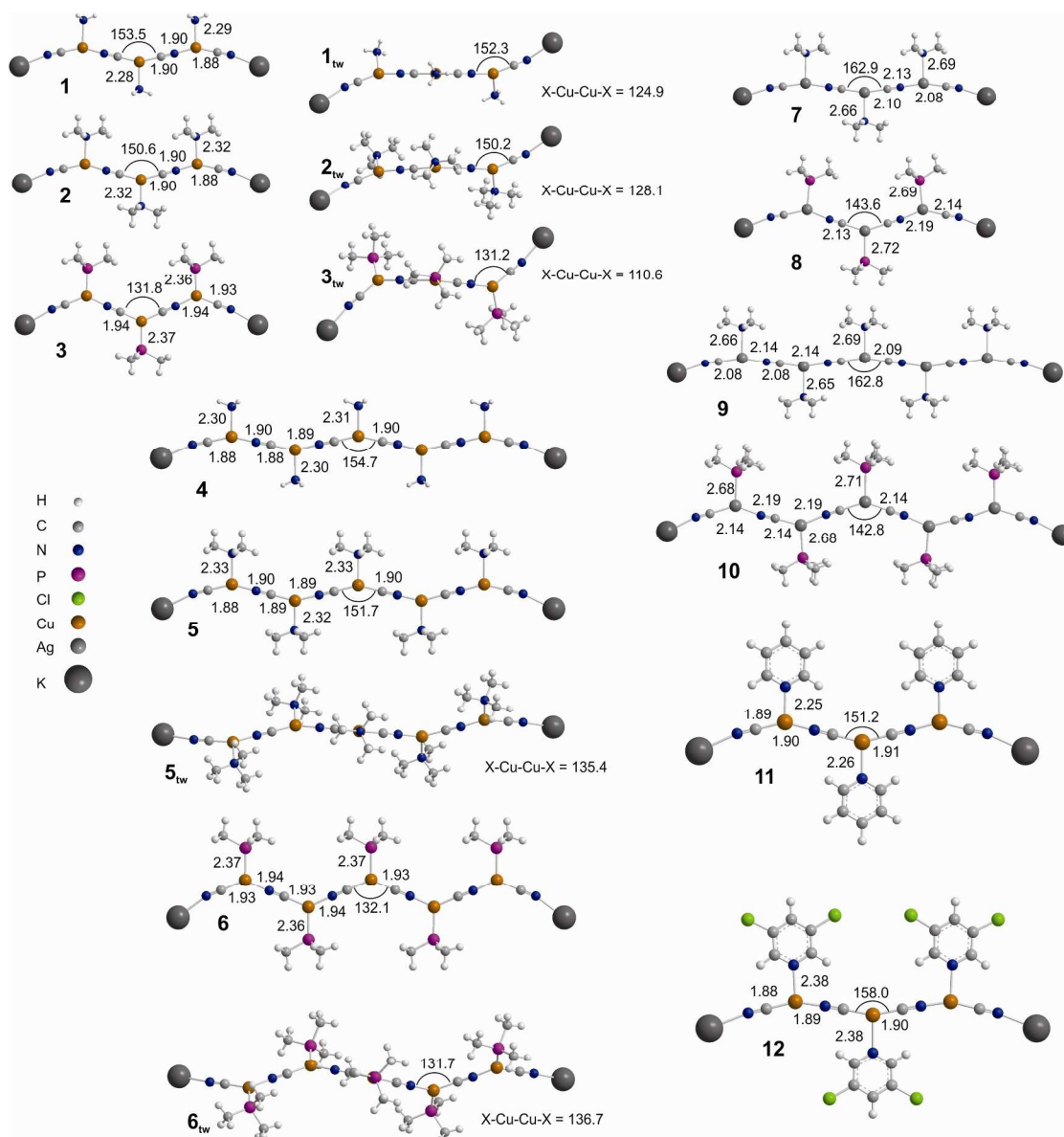


Fig.2 Selected DFT(BLYP)-optimized bond distances (Å) and angles (°) for the decorated MCN models $\{K_2[Cu_n(CN)_{n+1}(L)_n]\}^+$ ($n = 3$, $L = NH_3$ (1), NMe_3 (2), PMe_3 (3), Pyr (11) and 3,5- Cl_2 Pyr (12); $n = 5$, $L = NH_3$ (4), NMe_3 (5), PMe_3 (6)) and $\{K_2[Ag_n(CN)_{n+1}(L)_n]\}^+$ ($n = 3$, $L = NMe_3$ (7), PMe_3 (8); $n = 5$, $L = NMe_3$ (9), PMe_3 (10)). Bond distances and angles for the twisted models are similar to those of the planar zigzag.

In our previous study of $CuCN$,³⁴ and later $AgCN$ and $AuCN$,³² we used short lengths of the MCN coordination polymer capped by K^+ ions to model the electronic structure of the bulk material. Time-dependent DFT (TD-DFT) calculations on these chains showed that the excitation spectrum could be attributed to transitions between π -type MOs. The emission spectrum was consistent with the singlet-triplet (S-T) gap between the ground state and a non-linear excited state. The fact that the excited state contained a bend at one of the metal ions suggested that the shift into the visible region for decorated chains could be due to a reduction in reorganization energy as the system relaxes to the ground state. Further, the experimental excitation and emission spectra for MCN were in agreement with the theoretical wavelengths.³² In this study, we extend these models to examine the effect of amine- and phosphine-decoration of the MCN ($M =$

Cu , Ag) backbone using DFT methods to determine the changes in electronic structure that lead to the shift in emission wavelength.

25 Methods

Models of decorated $Cu(I)$ and $Ag(I)$ cyanide chains were optimized with Gaussian 09³⁵ at the DFT level using the BLYP³⁶⁻³⁸ exchange-correlation (xc) functional. Triplet geometries were optimized using unrestricted Kohn-Sham orbitals. Bond distances for linear ground-state MCN model species are consistent with other theoretical studies.³⁹ Various authors have shown that pure DFT methods perform better than hybrid methods for some extended π systems. In our study of $CuCN$ model systems,³⁴ various functionals were tested and BLYP was shown to produce

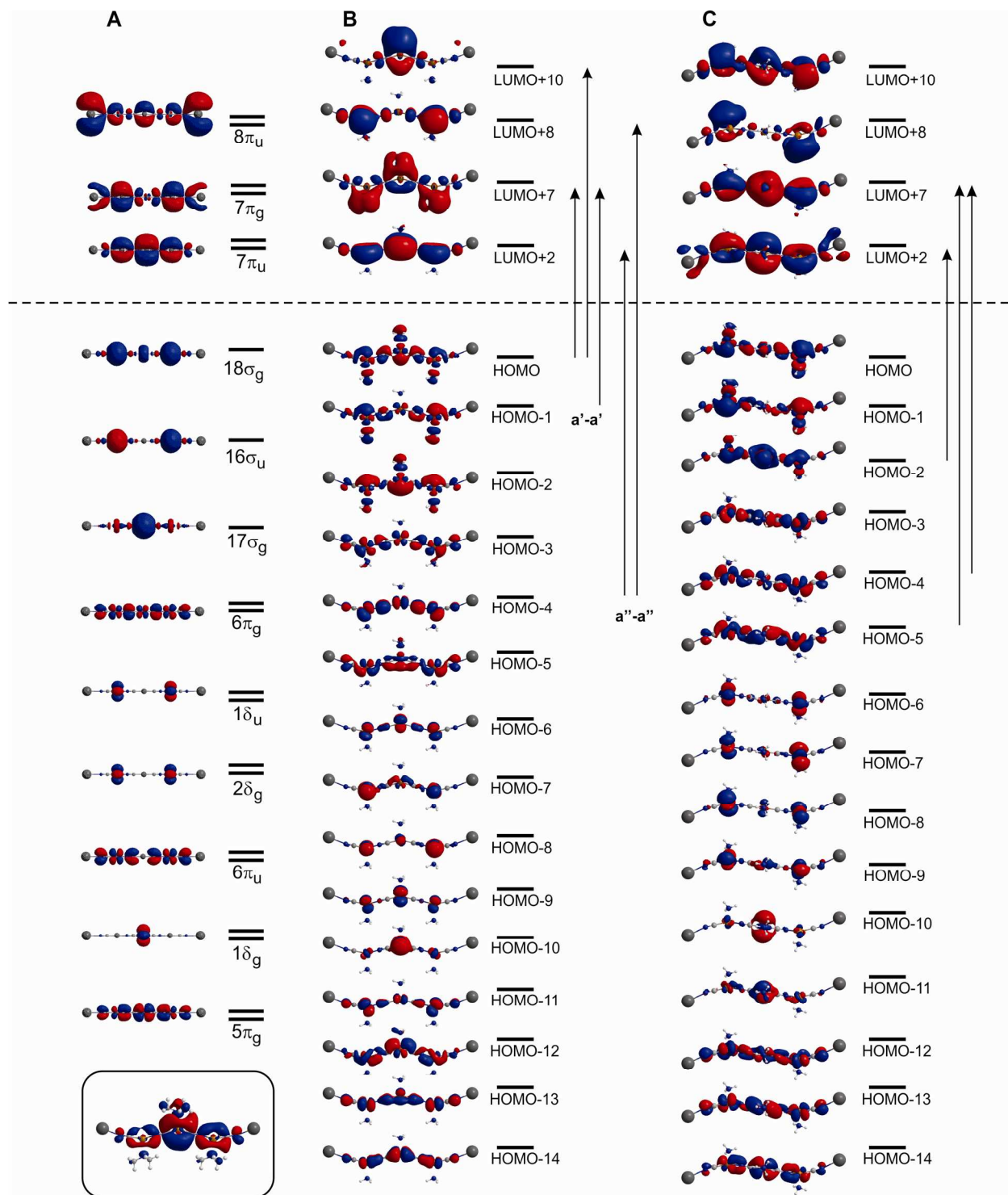


Fig. 3 Comparison of the MOs of the undecorated $\{K_2[Cu_3(CN)_4]\}^+$ (A), the planar zigzag NH_3 -decorated model **1** (B), and the twisted NH_3 -decorated model I_{tw} (C). Selected transitions that are predicted to contribute to the excitation spectrum are shown for **1** and I_{tw} . The inset shows the unoccupied MO of the NMe_3 -decorated model **2** equivalent to LUMO+7 in 3B.

the best agreement with experimental data. Although hybrid functionals produced reasonable bond distances within the model chains, the excitation energies calculated by TD-DFT for these functionals were consistently over-estimated relative to BLYP and other pure functionals.³⁴ Test calculations of the ammine-

decorated model chains presented in this study using the mPW1PW91 xc functional produced similar structures to the BLYP functional. The copper atoms were represented by the Ermler-Christiansen relativistic effective core potential (RECP) basis set⁴⁰ modified to include the 4p contractions of Couty and

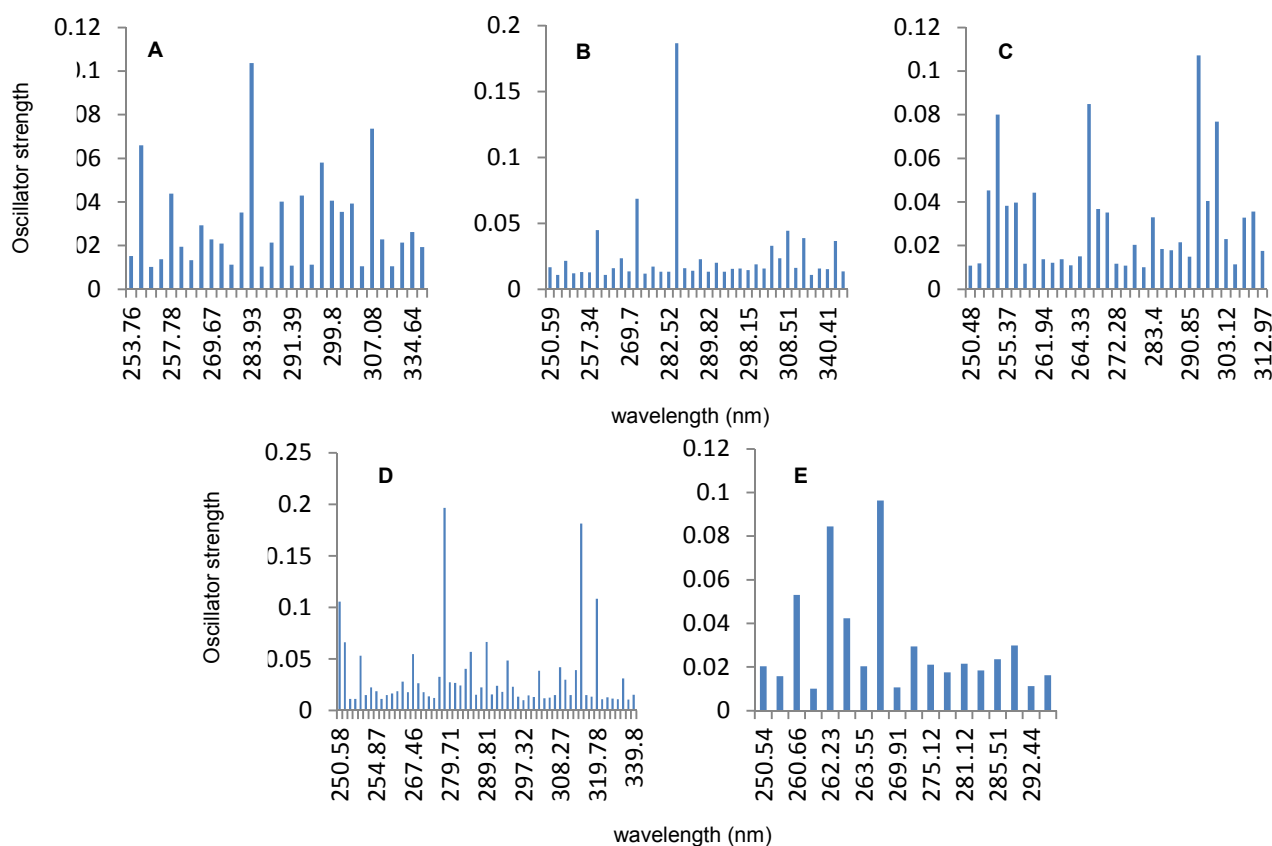


Fig. 4 Simulated excitation spectra (TD-DFT(BLYP)) for **1** (A), **1_{rw}** (B), **2** (C), **4** (D), and **7** (E). Transitions with oscillator strengths < 0.01 are omitted.

Hall.⁴¹ Basis sets for the carbon and nitrogen atoms of the MCN chain were the split-valence triple- ζ plus polarization functions (TZVP) representations of Dunning.⁴² Methyl groups were represented by the Dunning's double- ζ basis set.⁴³ The potassium atoms were represented by the Hay-Wadt RECP basis set. The excitation spectra of the model chains were simulated using TD-DFT to generate all singlet excitations up to 250 nm.

Results and Discussion

Models of MCN-L ($M = \text{Cu}, \text{Ag}; L = \text{NH}_3, \text{NMe}_3, \text{PMe}_3$). Short, decorated chains of $\{\text{K}_2[\text{Cu}_n(\text{CN})_{n+1}(\text{L})_n]\}^+$ ($n = 3, L = \text{NH}_3$ (**1**), NMe_3 (**2**), PMe_3 (**3**); $n = 5, L = \text{NH}_3$ (**4**), NMe_3 (**5**), PMe_3 (**6**)) were optimized as a planar zigzag structure (pseudo- C_{2v} (C_s) symmetry) with C-Cu-C and C-Cu-L angles constrained to be equal to prevent significant distortions in the CuCN backbone. These constraints result in deviations of less than 1 kcal/mol versus the fully-optimized C_s structure. Cyano ligands were oriented such that the carbon ends face the central Cu centre. The ends of the chains were capped by K^+ to maintain a symmetric environment and neutralize the negative charge of the $[\text{M}_n(\text{CN})_{n+1}]^-$ complex ions. Capping of the models with a cation was used to prevent underestimation of the electron binding energy known for anions within DFT, but may shift the excitation energies to shorter wavelengths due to the overall positive charge. Potassium was selected as the counterion because it is commonly

used as a mineralizing agent for CuCN.

The DFT-optimized structures (Fig 2) of **1-6** are generally consistent with the X-ray structure of the NEt_3 -substituted chain.²⁶ [Note that $\text{CuCN}(\text{NH}_3)$ is a known material that forms a 2D sheet through μ_3 -C,C,N-bridging of the cyano ligand.⁴⁴] The DFT Cu-NC bond distances (1.89–1.90 Å) are in agreement with those seen in the crystal structure (Cu-NC 1.892 Å; Cu-CN 1.865 Å; Cu- NEt_3 2.205 Å), but the Cu-CN (1.88 Å) and Cu- NH_3 (2.29–2.32 Å) distances are longer by 0.02–0.1 Å. The largest deviations are for the Cu-NR₃ distances which are more influenced by interactions between the chains within the solid material. The X-Cu-X bond angles (X designates either C or N on the MCN backbone) for **1** and **4** are slightly more obtuse relative to the X-ray structure for $\text{CuCN}(\text{NEt}_3)$ (148.9°)²⁶ and the NMe_3 -decorated model (150.3°) due to the lack of steric interactions between the R groups and the CuCN backbone. The stronger donating PMe_3 ligand led to greater distortions in the CuCN backbone, reducing the X-M-X bond angle to 131.8°. Cu-P bond distances are shorter than those found in the X-ray structures for CuCN substituted with PCy_3 .³¹ When the C_s constraint is removed, the CuCN-L chains tend toward a helical structure (e.g., **1_{rw}**) similar to that experimentally observed for Et_2NH -decorated CuCN (DFT: X-Cu...Cu-X 124.9°; exp: 123.6°).²⁶ The small energy difference between the planar zigzag and the helix formation (< 1 kcal/mol) is consistent with the influence of crystal packing forces on the conformation of the decorated

coordination polymers.¹⁰

For comparison, decorated AgCN chains $\{K_2[Ag_n(CN)_{n+1}(L)_n]\}^+$ ($n = 3$, $L = NMe_3$ (**7**), PMe_3 (**8**); $n = 5$, $L = NMe_3$ (**9**), PMe_3 (**10**)) were modelled using a similar approach (Fig 2). Unlike the CuCN models, the AgCN model chains prefer the zigzag structure and do not form helices. These Ag models have more obtuse angles ($X-Ag-X = 163^\circ$) along the backbone, potentially due to the greater stability of the Ag d^{10} orbitals. The more linear $X-Ag-X$ bond angles indicate that AgCN has less affinity than CuCN for the binding of additional ligands although coordination of the more basic PMe_3 decreases the angle to 143° . This weaker binding may explain why AgCN often forms materials in which every other metal centre is decorated. For example, the 1:1 product observed for AgCN and PCy_3 represents an unusual case in which the phosphine coordinates to alternate Ag(I) centres on a highly ordered $-Ag(PR_3)_2-NC-Ag-CN-$ backbone.³¹ The phosphines bond to the N-coordinated Ag(I) due to the weaker coordination of the isocyanide linkage. Thus, the polymer consists of $[Ag(PCy_3)]^+$ units bridged by dicyanoargentate(I) anions. A related $(PCy_3)_2Ag-NC-Ag-CN$ molecular form has also been synthesized.³¹

Models of the CuCN-L excitation and emission spectra. The excitation spectrum of MCN has been attributed to transitions from π -type MOs with antibonding character between M d_π AOs and π_{CN} fragments to unoccupied MOs with bonding character between M 4p AOs and π_{CN}^* fragments (Fig 3A).^{32,34} Because the occupied π -type MOs lie below the σ -type orbitals, the longest wavelength transitions are not HOMO-LUMO, but rather between the highest occupied π -type MOs and the lowest unoccupied π -type MOs (HO π MO-LU π MO). Upon coordination of the ammine ligands, these degenerate pairs of MOs split into sets of in-plane (A') and out-of-plane (A'') MOs with respect to the zigzag backbone (Fig 3B). For example, for the three-Cu model chain **1**, the degenerate MO pair $6\pi_g$ corresponds to HOMO-3 (a') and HOMO-4 (a''). In many cases, there is also a large degree of mixing of the MCN MOs due to the zigzag structure of the decorated chain. For example, HOMO-2 is a mixture of the π -character of $6\pi_g$ with the δ -character of $1\delta_u$. In forming the Cu-NH₃ bond, the ammine ligand donates electron density to the in-plane combination of unoccupied π -type MOs (e.g., $7\pi_u$) to form a bonding MO (not shown) and an antibonding MO (e.g., LUMO+7). Ammine-coordination destabilizes the backbone MOs to reduce the HOMO-LUMO+2 gap from 4.09 eV to 3.21 eV. [Note: In **1**, the LUMO and LUMO+1 are the K 4s AOs and are artefacts of the capped models. LUMO+3, 4, +5, +6 are K 4p-based (not shown).] In the NH₃-decorated chains, the in-plane π -type unoccupied MOs (i.e., LUMO+7) appear to be delocalized over the ligand, but this effect is attributed to the overlap of the backbone lobes with the hydrogens of the amine. The NMe_3 models more clearly show these MOs to have Cu-N antibonding character (see inset to Fig 3). The MOs of the twisted models retain many of the features of the zigzag structures, mixing the in- and out-of-plane lobes and localizing the MOs to the CuCN backbone, giving them an appearance more similar to that of undecorated CuCN (Fig 3C).

TD-DFT calculations on the model zigzag chains **1-6** show that the major transitions are red-shifted by 40-70 nm relative to

the CuCN models due to the destabilization of the π -type MOs through decoration of the chain (Fig 4). As the chain length increases from $n=3$ to 5, the wavelength of the excitations increases by ~ 20 nm, similar to what was observed for undecorated CuCN models.³⁴ The wavelengths of the excitations will approach a constant value as n is increased, but the trends in MO structure for these short models are expected to be consistent with those of the longer chains.

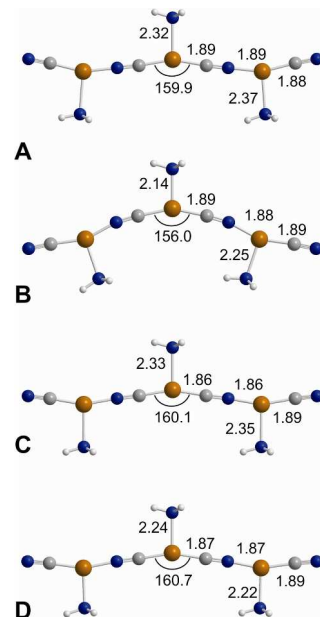


Fig. 5 Selected DFT(BLYP)-optimized bond distances (Å) and angles ($^\circ$) for (A) the ground state of **1**⁻, (B) the ³A' state arising from an $a' \rightarrow a'$ transition, (C) the ³A' state arising from an $a'' \rightarrow a''$ transition, and (D) the ³A'' state.

The principle excitations for **1-6** were characterized as those involving $a' \rightarrow a'$ and $a'' \rightarrow a''$ transitions between the in-plane and out-of-plane MOs localized on the CuCN backbone, respectively. Oscillator strengths, a measure of the intensity of an excitation, are generally one order of magnitude lower than the CuCN model chains.³⁴ The first significant transition for **1** is calculated to occur at 334 nm (Fig 4A) as the excitation from the HOMO to the lowest unoccupied a' MO (LUMO+7). The most intense transition (307 nm) corresponds to an excitation from the highest occupied to the lowest unoccupied a'' MOs (HOMO-4 to LUMO+2). Bending of the chain destabilizes the occupied π MOs in the plane of the chain so as to reduce the excitation energy. The twisted models tend to have a dominant excitation (HOMO-3(4) to LUMO+8) shifted to a shorter wavelength (284 nm). These results for **1** and **1**_{tw} are consistent with experimental studies of CuCN(NH₃) and CuCN(NH₂) for which λ_{max} is 315 and 290 nm, respectively.¹⁰ This blue-shifting of the helical structures can be attributed to the greater localization of the MOs to the CuCN backbone which stabilizes the highest occupied MOs and destabilizes the lowest unoccupied MOs to increase the band gap for helical chains. The character of the MOs that contribute to the transitions for the NMe_3 - and PMe_3 -decorated CuCN and AgCN model chains, as well as the longer $n=5$ chains, are consistent with the results for **1**. Additionally, as observed for undecorated AgCN models, the excitations for $\{K_2[Ag_n(CN)_{n+1}(L)_n]\}^+$ (**7-10**) are found at shorter wavelengths than the Cu(I)

models (Fig 4E).

The emission spectrum is assumed to originate from the relaxation of an excited state triplet state which results from intersystem crossing (ISC) from an excited state singlet.

5 Adiabatic singlet-triplet gaps were determined from the unrestricted DFT-optimized geometries of the triplet state relative to the ground-state singlet structures of uncapped $\mathbf{1}^-$ (constrained to C_s symmetry) and corrected for the zero-point vibrational energy ($\Delta E+ZPE$). The K^+ ions were removed due to the
10 interference of the low-lying artefact K-type virtual MOs in the calculation of the triplet states. The optimized structure of the ground state of $\mathbf{1}^-$ is similar to that of $\mathbf{1}$ (Fig 5), except that the X-Cu-X angles are more obtuse (159.9°) and NH_3 has a longer bond distance to Cu(I). Due to the lowering of symmetry resulting
15 from chain decoration, excitations can either be into unoccupied MOs that are in the plane of the CuCN chain ($a' \rightarrow a'$), or out of the plane ($a'' \rightarrow a''$). The MOs for the former transitions are antibonding with respect to the ligands, whereas the latter are very similar to those of the undecorated chain. The S-T gap for the
20 ${}^3A'$ ($a' \rightarrow a'$) state (380 nm) is lower in energy and red-shifted relative to the undecorated CuCN models (328 nm). The unpaired electrons occupy the MOs analogous to the HOMO and LUMO+7 for $\mathbf{1}$ (Fig 3B) consistent with low energy $a' \rightarrow a'$ excitations between MOs in the plane of the backbone (Fig 3).
25 The C-Cu-C central bond angle decreases to 156° , a 3° difference with respect to the ground state (Fig 4). In contrast, the bend in the CuCN model chains is more significant ($\sim 85^\circ$). The smaller difference in this angle for the decorated triplet is due to the constraints of 3-coordination and contributes to the longer
30 emission wavelength for the decorated triplets because there is less reorganizational energy. A higher energy ${}^3A'$ ($a'' \rightarrow a''$) state of $\mathbf{1}^-$ (343 nm) with unpaired electrons in MOs analogous to HOMO-4 and LUMO+2 in $\mathbf{1}$ (Fig 3B) originates from ISC from the excited state singlet resulting from transition from the highest
35 out-of-plane a'' MO to the lowest unoccupied a'' MO perpendicular to the zigzag plane. This excitation transfers electron density from an MO that is antibonding between the metal centres and the CN ligands to one that is bonding. As a result, the backbone X-Cu-X bond angles become more linear
40 (160.1°) in order to increase the overlap between copper and the X centres.

For the helical models, the triplet state optimizes to a planar zigzag structure similar that of the higher energy ${}^3A'$ state (Fig 4D), but with a lower S-T gap (423 nm). Further examination of
45 the possible triplet states of the planar zigzag structure showed that the unpaired electrons in this lower energy triplet were located in MOs analogous to LUMO+2 (a'') and a linear combination of HOMO and HOMO-1 (a') for $\mathbf{1}$ (Fig 3B), consistent with a ${}^3A''$ state. Although the $a' \rightarrow a''$ transition is
50 forbidden in C_s symmetry, vibrations or twisting upon excitation in the bulk materials could lower the symmetry to allow for relaxation of the ${}^3A'$ state to this lower energy triplet. The structure of the ${}^3A''$ species is similar to that of the high-energy ${}^3A'$ with a near linear CuCN backbone ($\angle X\text{-Cu-X} = 160.7^\circ$). The
55 S-T gap for relaxation of this species to the ground state is consistent with the low-energy emission observed in many aliphatic CuCN-L materials (~ 450 nm) including CuCN(NMe_3) (zigzag) and CuCN(NHMe_2) (helical).

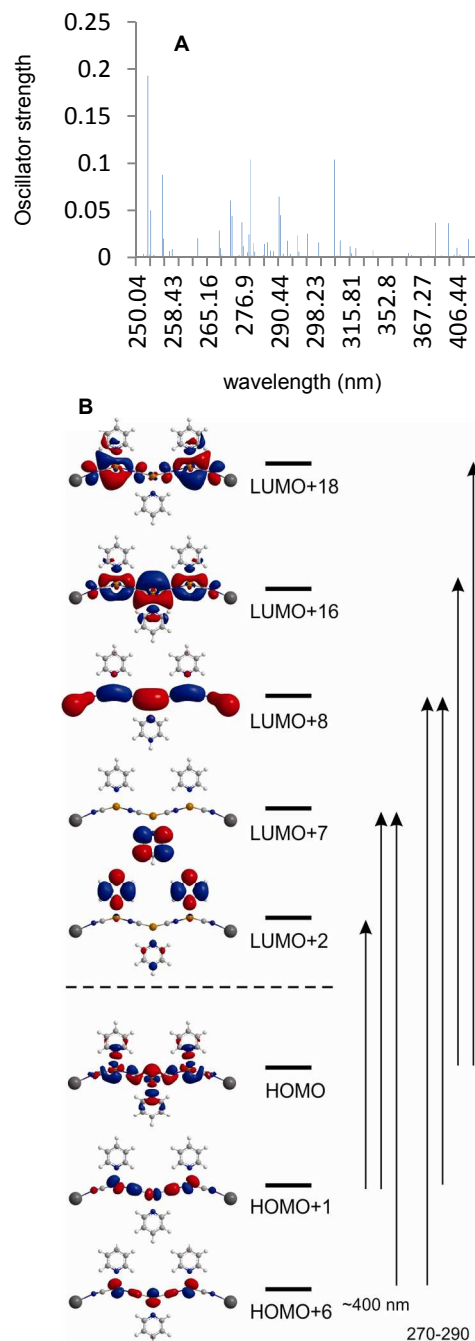


Fig. 6 (A) Simulated excitation spectra (TD-DFT(BLYP)) for $\mathbf{11}$; (B) Selected MOs and representative transitions for the Pyr-decorated model $\mathbf{11}$.

65 *Models of CuCN-L (L = Pyr, 3,5-Cl₂Pyr).* In order to explore the effect of decoration by aromatic ligands, we optimized short lengths of $\{\text{K}_2[\text{Cu}_n(\text{CN})_{n+1}(\text{L})_n]\}^+$ (L = Pyr, ($\mathbf{11}$) and 3,5-Cl₂Pyr ($\mathbf{12}$); Fig 2). The optimized structure in C_{2v} symmetry prefers a
70 planar zigzag with the Pyr rings planar with the CuCN backbone. Structures were also obtained by varying the dihedral angle for rotation about the Cu-N_{Pyr} bond between 0° to 90° . The energy required to twist the Pyr to 90° is low for either Pyr or 3,5-Cl₂Pyr (~ 4.5 kcal/mol). Experimental structures of Pyr-decorated CuCN

networks show that the Pyr ring is not coplanar with the CuCN chain due to steric interactions and crystal packing forces. The Cu–N_{Pyr} bond distance increases slightly for Pyr because it is twisted out of the plane of the CuCN backbone, but this distance increases by 0.1 Å for weaker 3,5-Cl₂Pyr ligand, due to the loss of delocalization of the backbone π system over the ring. Often more than one Pyr ligand coordinates to the metal centres. For CuCN(Pyr)₂⁴⁵ and (CuCN)₂(4-MePyr)₃, which maintain the roughly planar zigzag with decoration of the second equivalent of Pyr above the ring, the Cu(I) centres do not distort toward tetrahedral coordination, but bond out-of-plane at roughly 90° to the in-plane Pyr. In these materials, the second equivalent of Pyr ligands forms bonding interactions through the out-of-plane unoccupied MOs. The added ligands interact more weakly due to the preference for the in-plane Pyr to remain planar with the backbone, preventing steric interactions. The out-of-plane Pyr are also stabilized by CH $\cdots\pi$ interactions between the rings forming a herringbone configuration. Other 1:2 and 2:3 networks, such as CuCN(3-ClPyr)₂, CuCN(3-MeOPyr)₂, (CuCN)₂(2-MePyr)₃, and (CuCN)₂(3-EtPyr)₃, form more nearly tetrahedral arrangements along a helical backbone.¹⁰ Materials having more than one, but less than two L, per Cu alternate 3- and 4-coordination,⁷ probably due to steric interactions with the backbone and neighbouring groups preventing these CH $\cdots\pi$ interactions.

TD-DFT calculations were performed for each of the structures in which the dihedral angle for the Pyr was varied between 0 and 90°. The predicted excitation spectra are dominated by two features: a weak band at ~400 nm and a much stronger band starting at ~300 nm (Fig 6A). These bands are red-shifted for 3,5-Cl₂Pyr (415 and 350 nm, respectively). For the minimum 0° structure, the long wavelength band consists of excitation from out-of-plane π -type MOs on the CuCN backbone to the π^* of the Pyr ligands (A: $a_1 \rightarrow b_1$). At 90°, the excitation from an in-plane CuCN MO to a different Pyr π^* combination (B: $a_1 \rightarrow a_2$) contributes to the long wavelength excitation. At 0° angle, the former is symmetry allowed and the latter is forbidden, and vice versa at 90°. As the dihedral angle for twisting Pyr increases from 0°, the intensity of excitation A decreases as the dihedral increases and intermediate angles show contributions from both transitions. The change in the MO from which the electron is excited may affect the geometry of the resulting triplet. The shorter wavelength band consists of transitions between MOs localized on the CuCN backbone (Fig 6B). Etaiw et al. compared the excitation spectrum of 3,5-Cl₂Pyr to CuCN(3,5-Cl₂Pyr) in order to assign the bands as MLCT (285 and 310 nm) and CN ligand π - π^* (350 nm).²⁴ From the results of our model calculations, the major band observed experimentally is likely due to transitions between MOs on the CuCN backbone, with any MLCT transitions lying at higher wavelengths and being much lower in intensity. The low-energy (LE) emission feature observed in the emission spectra of many CuCN-L (L = aromatic amine) materials¹⁰ could be due either to transitions between different types of CuCN backbone MOs or ISC to a MLCT state which emits at a longer wavelength. The high energy (HE) emission bands are due to transitions on the CuCN backbone. In the experimental spectra, distinct LE excitation bands are not observed. The HE excitation band for (CuCN)₂(2MePyr)₃ was found to consist of two portions, producing separate emission

bands. However, these are the probable result of the two distinct coordination environments for Cu(I) within the chains. The results presented herein suggest that a true LE excitation band associated with MLCT to an aromatic ligand would probably be found at wavelengths >400 nm.

Conclusions

Decorating Cu(I) and Ag(I) with amines and phosphines alters both the geometry and electronic structure of MCN materials. The choice of zigzag versus helical structures for these materials is likely controlled by crystal packing forces and interactions between the ligands. The excitation spectra of these materials (whether zigzag or helical) are related to those of the undecorated MCN insofar as transitions are between π -type MOs are located on the backbone. The shifts in the wavelengths can be attributed to destabilization of the MOs upon coordination of the ligand. Contrary to our previous calculations for the simple {K₂[CuCN(Pyr)]}⁺ model,¹⁰ excitations for CuCN decorated with aromatic amines to π^* orbitals localized on the aromatic ring (MLCT) do not appear to contribute to the excitation spectrum of 1:1 CuCN materials with Pyr derivatives.

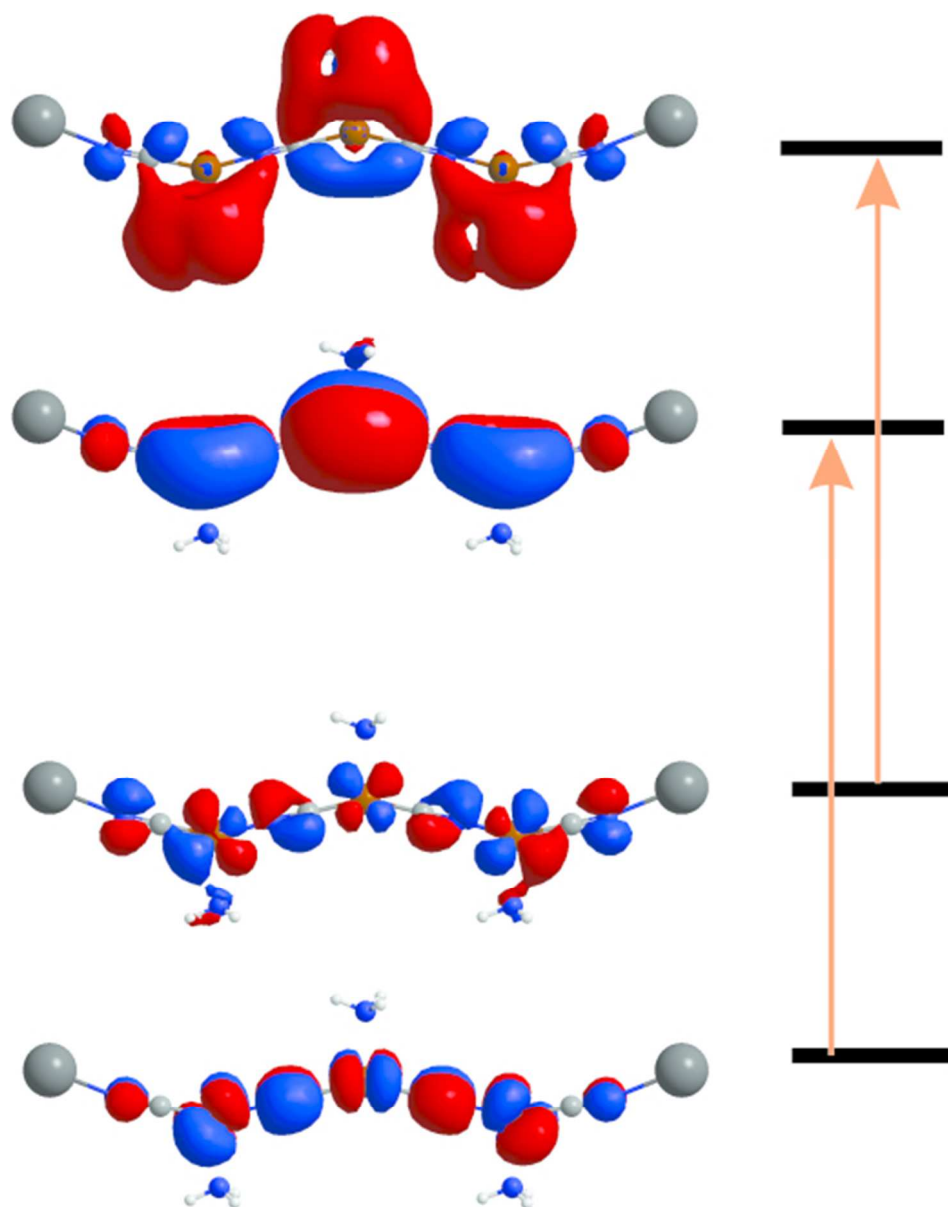
The drawback to modelling single chains is that the effect of steric interactions with nearby chains is omitted in the triplet calculations. These interactions should restrict significant changes in the chain structure. We would expect that the calculations, which allow more flexibility in the optimization of the structure, may overestimate the reorganization energy of the chains and give shorter wavelengths than are seen in the solid-state systems, especially for helical systems. Furthermore, the lack of M \cdots M interactions found in the solid-state for some materials can result in the omission of some spectroscopic features from our small models.⁴⁶ Nonetheless, the synergy between experimental spectroscopy, structure determination and DFT calculations on isolated model systems have proven to be highly successful for the prediction of luminescent properties of MCN and decorated MCN materials.

This work was funded by the National Science Foundation (CHE-0848109). J.L.M. thanks the Virginia Space Grant Consortium for an Undergraduate Research Scholarship.

Notes and references

- ^a Department of Chemistry and Biochemistry, Old Dominion University, Hampton Boulevard, Norfolk, VA 23529, USA. Fax: 01 757 683 4628; Tel: 01 757 683 4097; E-mail: cbayse@odu.edu
- ^b Department of Chemistry, College of William and Mary, Williamsburg, VA 23187-8795, USA. Fax: +757-221-2715; Tel: +757-221-2555; E-mail: rdpik@wm.edu
- S. J. Hibble, S. M. Cheyne, A. C. Hannon, and S. G. Eversfield, *Inorg. Chem.*, 2002, **41**, 4990–4992.
 - O. Reckeweg, C. Lind, A. Simon, and F. J. DiSalvo, *Z. Naturforschung*, 2003, **58B**, 155–158.
 - S. J. Hibble, S. G. Eversfield, A. R. Cowley, and A. M. Chippindale, *Angew. Chem. Int. Ed.*, 2004, **43**, 628–630.
 - S. J. Hibble, S. M. Cheyne, A. C. Hannon, and S. G. Eversfield, *Inorg. Chem.*, 2002, **41**, 1042–1044.
 - S. J. Hibble, A. C. Hannon, and S. M. Cheyne, *Inorg. Chem.*, 2003, **42**, 4724–4730.
 - G. A. Bowmaker, B. J. Kennedy, and J. C. Reid, *Inorg. Chem.*, 1998, **37**, 3968–3974.
 - R. D. Pike, *Organometallics*, 2012, **31**, 7647–7660.

8. T. A. Tronic, K. E. deKrafft, M. J. Lim, A. N. Ley, and R. D. Pike, *Inorg. Chem.*, 2007, **46**, 8897–8912.
9. M. J. Lim, C. A. Murray, T. A. Tronic, K. E. deKrafft, A. N. Ley, J. C. deButts, R. D. Pike, H. Lu, and H. H. Patterson, *Inorg. Chem.*, 2008, **47**, 6931–6947.
10. M. D. Dembo, L. E. Dunaway, J. S. Jones, E. A. Lepekina, S. M. McCullough, J. L. Ming, X. Li, F. Baril-Robert, H. H. Patterson, C. A. Bayse, and R. D. Pike, *Inorganica Chim. Acta*, 2010, **364**, 102–114.
11. R. D. Pike, T. M. Dziura, J. C. deButts, C. A. Murray, A. T. Kerr, and C. L. Cahill, *J. Chem. Crystallogr.*, 2014, **44**, 42–50.
12. G. A. Bowmaker, Effendy, J. C. Reid, C. E. F. Rickard, B. W. Skelton, and A. H. White, *J. Chem. Soc. Dalton Trans.*, 1998, 2139–2146.
13. G. A. Bowmaker, K. C. Lim, B. W. Skelton, and A. H. White, *Z. Naturforsch.*, 2004, **59B**, 1264–1276.
14. G. A. Bowmaker, R. D. Hart, B. W. Skelton, and A. H. White, *Z. Naturforsch.*, 2004, **59B**, 1293–1300.
15. G. A. Bowmaker, C. Pettinari, B. W. Skelton, N. Somers, N. A. Vigar, and A. H. White, *Z. Für Anorg. Allg. Chem.*, 2007, **633**, 415–421.
16. A. M. Chippindale, S. J. Hibble, and A. R. Cowley, *Inorg. Chem.*, 2004, **43**, 8040–8048.
17. S. J. Hibble and A. M. Chippindale, *Z. Für Anorg. Allg. Chem.*, 2005, **631**, 542–545.
18. S. E. H. Etaiw, S. A. Amer, and M. M. El-bendary, *Polyhedron*, 2009, **28**, 2385–2390.
19. S. E. H. Etaiw, S. A. Amer, and M. M. El-bendary, *J. Mater. Sci.*, 2010, **45**, 1307–1314.
20. S. E. H. Etaiw and M. M. El-bendary, *J. Inorg. Organomet. Polym. Mater.*, 2010, **20**, 739–745.
21. S. E. H. Etaiw, T. A. Fayed, and S. N. Abdou, *J. Inorg. Organomet. Polym. Mater.*, 2010, **20**, 326–333.
22. S. E. H. Etaiw, M. E. El-Zaria, T. A. Fayed, and S. N. Abdou, *J. Inorg. Organomet. Polym. Mater.*, 2011, **21**, 465–475.
23. S. E. H. Etaiw and S. N. Abdou, *J. Inorg. Organomet. Polym. Mater.*, 2013, **23**, 1296–1304.
24. S. E. H. Etaiw and M. M. El-bendary, *Spectrochim. Acta. A. Mol. Biomol. Spectrosc.*, 2013, **110**, 304–310.
25. O. Teichert and W. S. Sheldrick, *Z. Für Anorg. Allg. Chem.*, 2000, **626**, 1509–1513.
26. J. C. Dyason, P. C. Healy, L. M. Engelhardt, C. Pakawatchai, V. A. Patrick, and A. H. White, *J. Chem. Soc. Dalton Trans.*, 1985, 839–844.
27. Y.-B. Qiao, K.-F. Wang, L.-H. Hu, and F.-F. Jian, *Chin. J. Chem.*, 2006, **24**, 1144–1147.
28. M. Ghazzali, M. H. Jaafar, S. Akerboom, A. Alsalmeh, K. Al-Farhan, and J. Reedijk, *Inorg. Chem. Commun.*, 2013, **36**, 18–21.
29. G. A. Bowmaker, K. C. Lim, N. Somers, B. W. Skelton, and A. H. White, *Z. Naturforsch.*, 2004, **59B**, 1301–1306.
30. L. C. Yu, L. Lai, S. L. Liu, and Y. Xia, *Russ. J. Coord. Chem.*, 2010, **36**, 120–123.
31. Y.-Y. Lin, S.-W. Lai, C.-M. Che, Fu, Z.-Y. Zhou, and N. Zhu, *Inorg. Chem.*, 2005, **44**, 1511–1524.
32. C. A. Bayse, J. L. Ming, K. M. Miller, S. M. McCollough, and R. D. Pike, *Inorganica Chim. Acta*, 2011, **375**, 47–52.
33. A. Ley, L. Dunaway, T. Brewster, M. Dembo, T. Harris, F. Baril-Robert, X. Li, H. Patterson, and R. Pike, *Chem. Commun.*, 2010, **46**, 4565–4567.
34. C. A. Bayse, T. P. Brewster, and R. D. Pike, *Inorg. Chem.*, 2009, **48**, 174–182.
35. *Gaussian 09*, Gaussian, Inc., Wallingford, CT, 2009.
36. A. D. Becke, *Phys. Rev. A*, 1988, **38**, 3098–3100.
37. R. Colle and O. Salvetti, *Theor. Chim. Acta*, 1975, **37**, 329–334.
38. C. Lee, W. Yang, and R. G. Parr, *Phys. Rev. B*, 1988, **37**, 785–789.
39. P. Zaleski-Ejgierd, M. Patzchke, and P. Pyykko, *J. Chem. Phys.*, 2008, **128**, 224303.
40. M. M. Hurley, L. F. Pacios, P. A. Christiansen, R. B. Ross, and W. C. Ermler, *J. Chem. Phys.*, 1986, **84**, 6840–6853.
41. M. Couty and M. B. Hall, *J. Comput. Chem.*, 1996, **17**, 1359–1370.
42. T. H. Dunning, *J. Chem. Phys.*, 1971, **55**, 716–723.
43. T. H. Dunning, *J. Chem. Phys.*, 1970, **53**, 2823–2833.
44. D. T. Cromer, A. C. Larson, and R. B. Roof, *Acta Crystallogr.*, 1965, **19**, 192–197.
45. M. M. Olmstead, G. Speier, and L. Szabó, *Acta Crystallogr. C*, 1993, **49**, 370–372.
46. A. M. Chippindale, S. J. Hibble, E. J. Bilbe, E. Marelli, A. C. Hannon, C. Allain, R. Pansu, and F. Hartl, *J. Am. Chem. Soc.*, 2012, **134**, 16387–16400.



Ligand decoration shifts the excitation and emission spectra of coinage metal cyanides. DFT and TD-DFT calculations are used to identify the MOs involved the transitions that contribute to photoluminescence.
43x55mm (300 x 300 DPI)